PAPER

Check for updates

Study on the unsteady state oxidative coupling of methane: effects of oxygen species from O_2, surface lattice oxygen, and CO_2 on the C_{2+} selectivity†

Suji Yoon,‡[ab] Seoyeon Lim,‡[ab] Jae-Wook Choi,[a] Dong Jin Suh,[ac] Kwang Ho Song [iD][bc] and Jeong-Myeong Ha [iD] *[acd]

This study examined the effects of oxygen species on the unsteady-state oxidative coupling of methane (OCM) using a lengthy catalyst bed of $Na_2WO_4/Mn/SiO_2$. The reaction conditions, including the methane-to-oxygen ratio, ratio of feed gas dilution by N_2, quantity of catalyst, and feed flow rate were adjusted for the continuous flow fixed bed reaction system. While the O_2 gas initiated methyl radical formation from methane, the surface lattice oxygen atoms improved the dehydrogenation of paraffins to olefins without significant activation of methane. The addition of CO_2 as a mild oxidizing agent was also tested and slightly improved OCM selectivity with slightly lower methane conversion were observed.

1. Introduction

The vast reserves of natural and shale gas have led to global interest in converting methane, their major component, to valuable chemicals. The oxidative coupling of methane (OCM) can directly produce ethylene using oxidizing agents including oxygen gas at a high reaction temperature (>600 °C), and hence it is a promising way to use the highly stable methane as feedstock. The proposed mechanism for OCM is composed of parallel and consecutive heterogeneous and gas-phase reactions.[1] The catalyst surface activated by the co-fed oxygen produces methyl radicals by hydrogen abstraction from methane. The methyl radicals can then be converted to the desired ethane in the gas phase, or further oxidized to the undesired CO and CO_2. It was suggested that an industrially feasible OCM process can be developed if the C_{2+} products (hydrocarbons containing two or more carbon atoms) achieve a yield above 25% and a selectivity of 75–80%.[2–9]

Because there is a critical technological barrier for the selective formation of olefins and paraffins while suppressing

[a]Clean Energy Research Centre, Korea Institute of Science and Technology, Seoul 02792, Republic of Korea. E-mail: jmha@kist.re.kr

[b]Department of Chemical and Biological Engineering, Korea University, Seoul 02841, Republic of Korea

[c]Graduate School of Energy and Environment (Green School), Korea University, Seoul 02841, Republic of Korea

[d]Division of Energy and Environment Technology, KIST School, Korea University of Science and Technology, Seoul 02792, Republic of Korea

† Electronic supplementary information (ESI) available. See DOI: 10.1039/d0ra06065h

‡ These authors equally contributed to this work.

the deep oxidation of methane to CO and CO_2,[6,8,10] many selective oxidation catalysts have been prepared for the OCM reaction. For unpromoted oxides of alkali, alkaline-earth, and rare earth metals, low CH_4 conversion and high C_{2+} selectivities were observed, along with lower C_{2+} yields (<12%),[11] although moderate OCM activity was achieved at lower reaction temperatures (<750 °C).[12] Perovskites, which are well-defined crystalline mixed oxides containing two different metals, were also used for catalyzing OCM,[13–15] exhibiting improved activity with promoter addition.[1,12] Among them, $Na_2WO_4/Mn/SiO_2$ is one of the most effective and stable OCM catalysts.[9,16–21] An optimized catalyst, composed of 2 wt% Mn and 5 wt% Na_2WO_4 on SiO_2, has exhibited ~25% C_{2+} yield.[6] The remarkable long-term stability of $Na_2WO_4/Mn/SiO_2$ (1000 h) was also reported for continuous-flow reactions.[21] Although the origin of its high catalytic activity has not yet been elucidated,[22] the unusual formation of α-cristobalite SiO_2 phase during calcination at 750–850 °C has been reported as a distinguishing feature of a good catalyst,[23] and the active species has been suggested to be Na^+ or Na_2WO_4 on silica surface with distorted WO_4^{2-} tetrahedra formed during phase transition.[23–25] In addition to the roles played by Na_2WO_4, manganese oxide was reported to improve the oxygen mobility via reduction of Mn^{3+} to Mn^{2+}.[26] Because of the proposed oxygen activation by Mn in the Na–O–Mn composites,[27] the selective formation of ethylene, which can occur by oxidative or non-oxidative dehydrogenation of ethane, can be controlled by tuning the surface Mn concentration.[24,28] Improved OCM activity by the addition of several additives to $Na_2WO_4/Mn/SiO_2$ has also been reported.[9,29]

Although a number of selective catalysts have been developed, a better understanding of the reaction conditions is also

required to achieve a feasible OCM process. Because of the limited supply of O_2 and the high CH_4 conversion through the reactor, in which a reactant mixture flows downward through the catalyst bed, the conditions including reactant compositions in the upper catalyst bed may be significantly different from those in the lower catalyst bed. When methane and oxidant are flown through the oxygen-rich top bed, the oxidant (mostly O_2) can be adsorbed on the catalyst surface. The adsorbed oxygen species activates methane by abstracting H to form methyl radicals, which are coupled to form ethane. In the oxygen-deficient bottom layer, methyl radicals, C_{2+} products, and carbon oxides are present and can interact with the unreacted methane and oxidant. The unreacted O_2 can activate methane by either forming methyl radical or deeply oxidize the highly active C_{2+} products to CO and CO_2, thereby decreasing the C_{2+} selectivity. The amount of initially supplied oxidants also influences the level of deep oxidation products in the bottom layer.

By using less-active oxidizing agents, including H_2O and CO_2, the selectivity of OCM products can be improved by suppressing the burning of valuable hydrocarbons to form CO and CO_2.[30] Water as an oxidant improved the coupling selectivity over perovskite catalysts, exhibiting increased C_2 production with increasing partial pressure of steam.[31] CO_2 has also been suggested as an alternative oxidant to O_2.[32–37] The formation of surface lattice oxygen atoms from CO_2 has been observed on PbO–MgO and PbO–CaO catalysts, which improves the abstraction of hydrogen atoms from methane.[32,35] In Na_2WO_4/ Mn/SiO_2, the presence of CO_2 caused structural modification to improve catalytic activity.[38] The formation of hot spots, which accelerate the deep oxidation to CO and CO_2 because of significant local exothermic reaction, was observed in the catalyst bed of a bench-scale OCM reactor,[39] and these hot spots can be reduced by the presence of CO_2 with high heat capacity.[40] In addition to the improved OCM activity, the presence of CO_2 stabilized the lithium-doped MgO catalyst and suppressed its deactivation.[36] For oxidative dehydrogenation, it was suggested that CO_2 improves selective OCM and stabilizes the catalysts by poisoning the nonselective active sites.[41]

The goal of this study is to understand the local OCM reaction throughout the catalyst bed under continuously changing reaction conditions, which can be attributed to the limited supply of oxidizing reagents (particularly O_2) in the fixed bed system. The temperature (750–850 °C), N_2 dilution ratio, CH_4/O_2 ratio, catalyst bed thickness, total feed flow rate, and the co-feeding rate of CO_2 were varied to study the behaviors of reactants and products under these continuously changing conditions. The effects of O_2 and CO_2 (as strong and mild oxidizing reagent, respectively) on the local OCM reaction were investigated in a long fixed bed system, which is meant to simulate possible scaled-up reactors. CO_2 as a mild oxidizing reagent can also function as a diluent in the OCM process, and it can be recycled with the unreacted methane in the industrial scale process. With continuous consumption of O_2 throughout the long catalyst bed and the formation of O_2-deficient region, the roles of lattice oxygen atoms on the OCM were also observed. Although a steady state was not achieved while the lattice

oxygen atoms were being consumed for the OCM, the unsteady state reaction examined here is useful for understanding the OCM reaction using lattice oxygen atoms. The spent catalysts were characterized using X-ray diffraction (XRD), X-ray photoelectron spectroscopy (XPS), and Raman spectroscopy to reveal changes in the catalysts during the OCM reaction.

2. Experimental

2.1. Materials

All chemicals were used without further purification. Sodium tungstate dihydrate ($Na_2WO_4 \cdot 2H_2O$, 99+%) was purchased from Yakuri Pure Chemicals (Kyoto, Japan). Manganese nitrate hexahydrate ($Mn(NO_3)_2 \cdot 6H_2O$, 98%) was purchased from Kanto Chemical (Tokyo, Japan). Silica gel (SiO_2, 60–325 mesh, 99.5%) was purchased from Johnson Matthey (Royston, United Kingdom). Manganese(II) tungsten oxide ($MnWO_4$, 99.9%) was purchased from Alfa Aesar (Haverhill, Massachusetts, USA). Manganese(III) oxide (Mn_2O_3, 99.9%) was purchased from Sigma-Aldrich (St. Louis, Missouri, USA). Methane (CH_4, 99.95%), oxygen (O_2, 99.995%), nitrogen (N_2, 99.9%), and carbon dioxide (CO_2, 99.99%) were purchased from Shinyang Sanso (Seoul, Korea). DI water (18.2 MΩ m) was prepared using an aquaMAX-Ultra 370 series water purification system (Young Lin Instruments, Anyang, Korea).

2.2. Catalyst preparation

The catalyst containing 5 wt% Na_2WO_4 and 2 wt% Mn on SiO_2 ($Na_2WO_4/Mn/SiO_2$) was prepared using a mixed slurry method.[39,42] Silica gel (28 g) was mixed with DI water (150 mL) and stirred at 105 °C for 1 h under reflux. $Mn(NO_3)_2 \cdot 6H_2O$ (3.146 g) dissolved in DI water (10 mL) and $Na_2WO_4 \cdot 2H_2O$ (1.684 g) dissolved in DI water (10 mL) were added drop-wise to the boiling mixture using a syringe pump over 15 min. The prepared thick paste was dried in air at 105 °C for 16 h and then calcined in air at 800 °C for 5 h. Prior to the reaction, the prepared catalyst powder was passed through 70–140 mesh.

2.3. Catalytic activity measurement

The catalytic reaction was performed using a fixed bed cylindrical quartz reactor (ID = 6 mm, length = 370 mm) (Fig. S1†). The unreacted O_2 leaving the catalyst bed can contribute to further homogeneous oxidation of the C_{2+} products to CO and CO_2 before the product mixture was inactivated by cooling,[38] which hinders interpretation of the reaction results. To reduce homogeneous reaction of the product mixture, a narrow exit was introduced on the reactor to encourage its fast outflow. The outlet of the reactor was narrower than the inlet (1 vs. 6 mm). The catalyst bed was located at the center of the reactor, with quartz wool placed at its upper and lower ends. $ZrSiO_4$ beads (Cenotec, Co. Ltd.) were positioned on the top of the catalyst bed to minimize the homogeneous reactions. A reaction mixture of CH_4, O_2, N_2, and CO_2 flowed into the catalyst bed. Notably, the furnace temperature, which was used as the reaction temperature in this study, was controlled (Fig. S2†). The measured temperature of catalyst bed was 0–40 °C higher, depending on the position in the

catalyst bed and the reaction conditions. The temperature measured at the bottom of catalyst bed was closest to the furnace temperature. Because the change of temperature though the catalyst bed was similar at each reaction temperature, we used the furnace temperature as the reaction temperature for convenience. Gas hourly space velocity (GHSV) was adjusted using catalyst bed volume and reactant flow rate. Water formed during the OCM reaction was removed at a cold trap ($-2\ ^\circ$C) connected to a chiller (VTRC-620, Jeio Tech). After an hour of isothermal operation, the product mixture was collected and analyzed using a thermal conductivity detector (TCD) and a flame ignition detector (FID) installed onto an online-gas chromatography system (Agilent 7890A). CH_4, O_2, N_2, CO, and CO_2 were analyzed using the TCD with a Carboxen 1000 column (Supelco, 60–80 mesh, 4.6 m $\times$ 1/8 in $\times$ 2.1 mm), and the hydrocarbons were analyzed using the FID with an HP-PLOT Al_2O_3 S capillary column (50 m $\times$ 320 μm $\times$ 8 μm). The catalytic performance was characterized by the following parameters:

$$CH_4\ \text{conversion}\ (X(CH_4), \%) = \frac{\text{moles of } CH_4 \text{ consumed}}{\text{moles of } CH_4 \text{ in the feed}} \times 100$$

$$\text{Selectivity to compound i}\ (S(i), \%) = \frac{\text{number of carbon atoms per compound i molecule} \times \text{moles of compound i}}{\text{moles of } CH_4 \text{ consumed}} \times 100$$

$$C_{2+}\ \text{selectivity}\ (S(C_{2+}), \%) = \frac{2 \times \text{moles of } C_2 \text{ hydrocarbons} + 3 \times \text{moles of } C_3 \text{ hydrocarbons}}{\text{moles of } CH_4 \text{ consumed}} \times 100$$

$$O_2\ \text{conversion}\ (X(O_2), \%) = \frac{\text{moles of } O_2 \text{ consumed}}{\text{moles of } O_2 \text{ in the feed}} \times 100$$

$$C_{2+}\ \text{yield}\ (Y(C_{2+}), \%) = \frac{CH_4 \text{ conversion} \times C_{2+} \text{ selectivity}}{100}$$

Table 1 Reactions during the OCM process

Reaction
CO production: $CH_4 + \frac{3}{2}O_2 \rightarrow CO + 2H_2O$
CO_2 production: $CH_4 + 2O_2 \rightarrow CO_2 + 2H_2O$
C_2H_6 production: $CH_4 + \frac{1}{4}O_2 \rightarrow \frac{1}{2}C_2H_6 + \frac{1}{2}H_2O$
C_2H_4 production: $CH_4 + \frac{1}{2}O_2 \rightarrow \frac{1}{2}C_2H_4 + H_2O$
C_3H_8 production: $CH_4 + \frac{1}{3}O_2 \rightarrow \frac{1}{3}C_3H_8 + \frac{2}{3}H_2O$
C_3H_6 production: $CH_4 + \frac{1}{2}O_2 \rightarrow \frac{1}{3}C_3H_6 + H_2O$

$$\text{Olefins/paraffins(mol/mol)} =$$

$$\frac{\text{moles of ethylene and propylene produced}}{\text{moles of ethane and propane produced}}$$

O_2-consumption for product i, the fraction of O_2 in the feed required to convert CH_4 into each product component i, was obtained using the following relationship described in Table 1:

2.4. Catalyst characterization

XRD results were collected to observe the catalysts' crystal structures using a Shimadzu XRD-6000 device equipped with a CuKα$_1$ ($\lambda = 0.15406$ nm) source. Raman spectroscopy analysis was performed using a Renishaw InVia Raman microscope. The surface electronic structures were analyzed using a PHI 5000 Versa Probe X-ray photoelectron spectroscope at Korea Basic Science Institute (Busan, Korea). The XPS spectra were calibrated using C 1s peak at 284.6 eV.

$$O_2\text{-consumption for compound i}\ (O_2\text{-cons.}(i), \%) =$$

$$\frac{S(i) \times \text{moles of } O_2 \text{ molecules to convert } CH_4 \text{ to compound i}}{S(CO) \times \frac{3}{2} + S(CO_2) \times 2 + S(C_2H_6) \times \frac{1}{4} + S(C_2H_4) \times \frac{1}{2} + S(C_3H_8) \times \frac{1}{3} + S(C_3H_6) \times \frac{1}{2}} \times 100$$

3. Results and discussion

3.1. Effects of CH_4/O_2 ratio and N_2 dilution on catalysis

Before investigating the effects of reaction conditions on the OCM results, the effects of O_2 concentration or the CH_4/O_2 ratio on the OCM activity were studied. $CH_4/O_2 = 3$ mol/mol was selected as an optimal reaction condition in this study because of the high C_{2+} selectivity with moderate CH_4 conversion, although the highest C_{2+} yield was not achieved using this ratio (Fig. 1 and Table S1†). Notably, in this study, C_{2+} compounds include ethane, ethylene, propane, and propylene. When CH_4/O_2 was adjusted from 1 to 6 mol/mol at 800 °C, the highest C_{2+} yield of 21.5% (44.0% CH_4 conversion and 49.0% C_{2+} selectivity) was achieved at 800 °C when $CH_4/O_2 = 2$ mol/mol. The C_{2+} selectivity sharply increased with increasing CH_4/O_2 ratio up to 3 mol/mol, and then steadily increased. Based on these observations, we selected $CH_4/O_2 = 3$ mol/mol for the good CH_4 conversion and high C_{2+} selectivity. The observed increase in C_{2+} selectivity and decrease in CH_4 conversion at a higher CH_4/O_2 ratio (i.e., reducing the limited supply of oxygen reactant) were consistent with the results of previous studies.[43] At higher CH_4/O_2 ratios, the amount of O_2 was insufficient for activating the large number of methane molecules, thus the CH_4 conversion decreased. At lower CH_4/O_2 ratios, the formation of methyl radicals was improved by the high partial pressure of O_2 to achieve high CH_4 conversion, but the methyl radicals were also easily oxidized to CO and CO_2 to decrease the C_{2+} yield (Table S1†). These observations suggest that a moderate CH_4/O_2 ratio is required to achieve a high C_{2+} yield by combining the CH_4 conversion and C_{2+} selectivity.
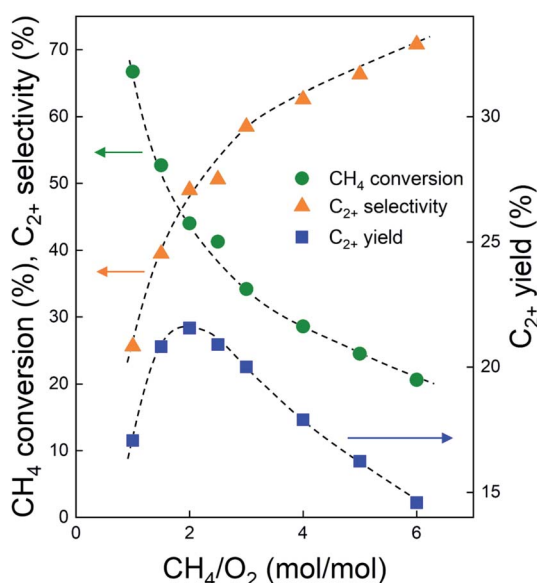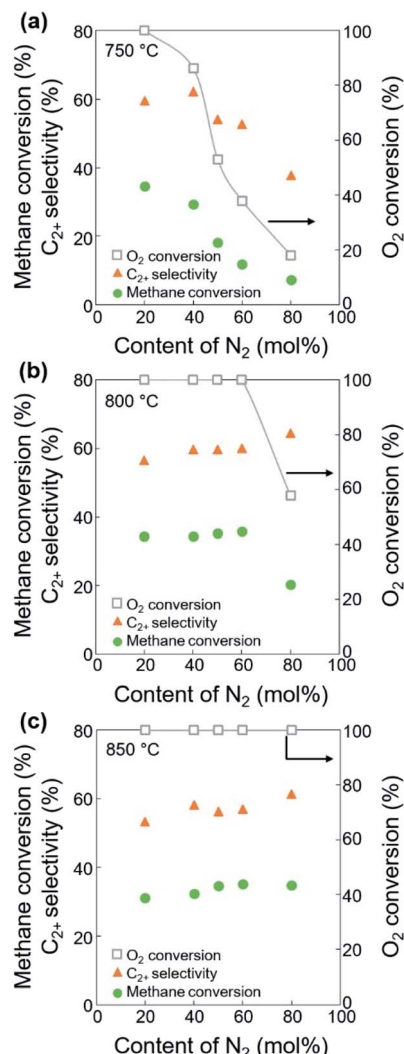

Fig. 2 CH_4 conversion (circles), C_{2+} selectivity (triangles), and O_2 conversion (squares) using different contents of N_2 diluent at (a) 750 °C, (b) 800 °C, and (c) 850 °C. CH_4/O_2 ratio = 3 mol/mol, GHSV = 10 000 h^{-1}.

Fig. 1 CH_4 conversion (circles), C_{2+} selectivity (triangles), and C_{2+} yield (rectangles) over $Na_2WO_4/Mn/SiO_2$ catalyst at 800 °C and different CH_4/O_2 (mol/mol) ratios. The O_2 conversions were 100% for all cases. GHSV = 10 000 h^{-1}. CH_4 flow rate was fixed at 18 mL min^{-1}, and the flow rates of O_2 and N_2 were adjusted to achieve the total flow rate of 50 mL min^{-1}.

With the CH_4/O_2 ratio fixed at 3 mol/mol, an optimized N_2 dilution ratio of 20% (v/v) or $CH_4/O_2/N_2 = 3/1/1$ mol/mol/mol produced the best CH_4 conversion and C_{2+} selectivity (Fig. 2 and Table S2†). High concentrations of methane and O_2 can accelerate the reaction rates, and the deep oxidation of methane to CO and CO_2 may occur along with the formation of hot spots because of the large heat of reaction.[39] Diluting the reactant mixture decreases the partial pressures of methane and O_2 and thus improves the selectivity for coupled C_{2+} hydrocarbons while suppressing the formation of CO and CO_2.[39,44,45] This change in the OCM results was more significant at the higher temperatures of 800–850 °C (with CH_4 conversions > 20%) and less significant at 750 °C (with CH_4 conversions < 20%). When the feed was highly diluted at the low reaction temperature, the formed methyl radicals may not be able to undergo gas-phase coupling with other methyl radicals in the highly diluted environment, which may reduce the C_{2+} selectivity. The general
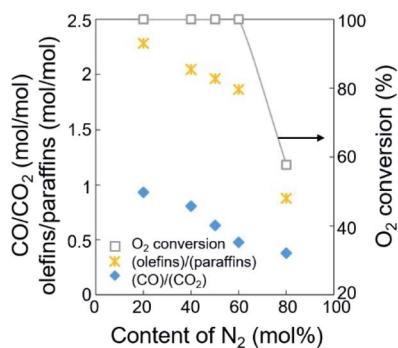
Fig. 3 Ratios of olefins/paraffins and CO/CO_2 for the dehydrogenation of paraffins and the oxidation of CO, depending on the content of N_2 diluent at 800 °C.

trend of increasing C_{2+} selectivity with increasing CH_4 conversion, under different reaction conditions for the same catalysts, has also been observed in our previous studies.[46–48]

The ratios of CO/CO_2 and olefins/paraffins increased at lower dilution by N_2 or higher partial pressures of the reactants (Fig. 3, S3, and Table S2†). Because higher partial pressures of the reactants are expected to improve the formation of CO_2 and increase the olefins/paraffins ratio,[44] the improved formation of CO rather than CO_2 we observed must come from another reaction pathway, which will be discussed later in the Section 3.2. Note that the amount of O_2 required for forming CO_2 is 1.33 times larger than that for forming CO, and the production of olefins from methane requires more than twice the amount of O_2 required to produce paraffins. Because of the limited supply of O_2 in this study, the deep oxidation to CO and CO_2 consumed more O_2 and suppressed the methane activation and the dehydrogenation, and this lowered the olefins/paraffins ratio.

3.2. Effects of catalyst bed thickness and feed flow rate on catalysis

Using the fixed CH_4/O_2 ratio and N_2 dilution, the effects of oxygen species on the OCM activity were investigated. The oxygen species activating methane and other hydrocarbons change throughout the long catalyst bed at a fixed flow rate. Both O_2 gas and surface oxygen species contribute to OCM, while only the latter are present at the O_2-deficient bottom part of the bed. With increasing catalyst bed thickness and the same flow rates of reactants, along with increasing residence time and decreasing GHSV, the reaction results did not significantly change when the O_2 was completely converted (Fig. 4a, c, S4, Tables S3 and S4†). While incomplete conversion of O_2 was observed at lower GHSV and lower reaction temperature, the 100% O_2 conversion produced almost the same CH_4 conversion (32.1–35.9%) along with 50.9–59.8% C_{2+} selectivity and 16.8–20.5% C_{2+} yield. The negligible C_{2+} production and CH_4 conversion in the O_2-deficient region (when 100% O_2 conversion was reached) indicated that the O_2 gas was required for significant conversion of methane to the C_{2+} compounds. Compared to the smaller changes in CH_4 conversion and C_{2+} selectivity, the olefin selectivity increased with increasing catalyst bed thickness, indicating that the olefins were formed by the oxidative dehydrogenation of paraffins at the O_2-deficient region. Based on these observations, the oxidative dehydrogenation of paraffins to olefins can be initiated by the surface lattice oxygen atoms. In contrast, the production of methyl radicals that contributed to CH_4 conversion was less initiated by these surface lattice oxygen atoms because there was no significant increase of CH_4 conversion at the O_2-deficient region. Therefore, the surface lattice oxygen atoms, which were formed by diffusion of bulk lattice oxygen atoms to the catalyst surface, mainly dehydrogenated the paraffins to olefins. Meanwhile, the surface-adsorbed oxygen atoms from the bulk O_2 gas preferentially converted methane to methyl radicals, which were further coupled to produce paraffins. In addition to the formation of olefins, the production of CO_2 also slightly increased with increasing catalyst bed thickness, indicating that dehydrogenation using surface lattice oxygen species was accompanied by deep oxidation to form CO_2 as by-product.

The OCM was also studied at a fixed catalyst bed thickness (0.18 mL or 6.4 mm) and adjustable feed flow rates (15–90 mL min⁻¹) to confirm the role of each oxygen species at $CH_4/O_2/N_2 = 3/1/1$ mol/mol/mol (Fig. 4b, d, S5, Tables S5 and S6†). When 100% O_2 conversion was achieved, the CH_4 conversion (28.5–35.5%) and C_{2+} selectivity (56.5–64.2%) were not significantly adjusted at 800–850 °C, indicating no significant dependence of OCM activity on the feed flow rate.

While the dehydrogenation of paraffins to olefins occurred at the O_2-deficient region using surface lattice oxygen species, as depicted in Fig. 4 and Table S3,† decreasing the feed flow rate, which has the same effect as increasing the catalyst bed thickness at a the fixed flow rate, did not significantly affect the dehydrogenation activity (Table S5†). A turbulent flow in the catalyst bed may suppress formation of the O_2-deficient region, obscuring the effects of surface lattice oxygen species.
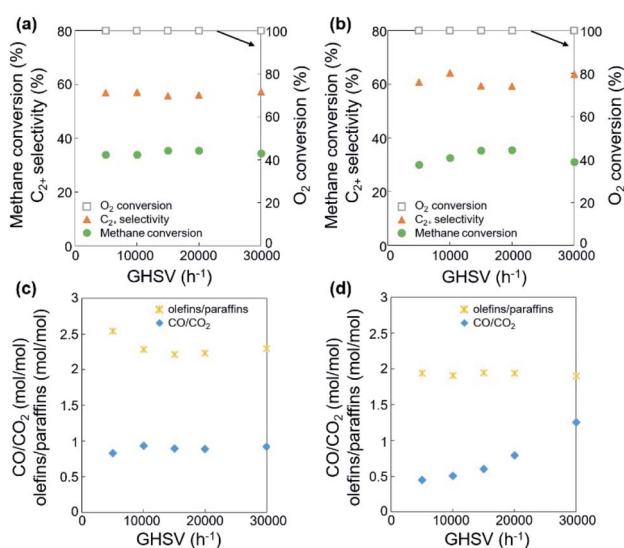

Fig. 4 (a and b) Catalytic activities and (c and d) ratios of olefins/paraffins and CO/CO_2 for the dehydrogenation of paraffins and the oxidation of CO, depending on the catalyst bed thickness (a and c) and feed flow rate (b and d) at 800 °C.
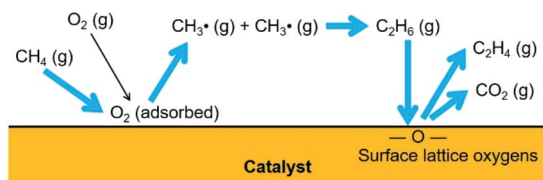
Fig. 5   Reactions by oxygen species.

In addition to dehydrogenation, the preferred formation of CO_2 over CO was observed, which indicates deeper oxidation to CO_2 at a lower GHSV, lower feed flow rate, or longer residence time. Particularly at 850 °C, the CO/CO_2 ratio significantly decreased at lower feed flow rate or longer residence time (Table S5†). The improved formation of CO_2, which consumed a large quantity of oxygen species, also reduced the CH_4 conversion because of the lack of oxidizing reagents. The preferred formation of CO at a shorter residence time can be attributed to the gas-phase formation of CO from methyl radicals.[5,49] CO can be preferentially produced when a methyl radical reacts with O_2 instead of another methyl radical, increasing the CO/CO_2 ratio.

The reactions preferred by the adsorbed O_2 and the surface lattice oxygen species are depicted in Fig. 5. Methane molecules were activated by the surface-adsorbed O_2 to form methyl radicals, which were then coupled to ethane. Ethane molecules were oxidatively dehydrogenated by the surface lattice oxygen species to form ethylene. The activation of methane molecules to methyl radicals by the surface lattice oxygen species was negligible; however, the dehydrogenation of paraffins and deep oxidation of hydrocarbons can be preferred by the surface lattice oxygen species.

3.3.   Effects of the catalyst bed thickness on the catalysis with co-fed CO_2

Based on the improved formation of CO_2 at lower feed flow rates, we studied the effects of a mild oxidant such as CO_2 on the OCM selectivity (or the product distributions of paraffins, olefins, CO, and CO_2). As one of the products of OCM, CO_2 can act as a diluent or a mild oxidant replacing the diluent N_2 and the oxidant O_2.[36,38,50] As a mild oxidant, a moderate concentration of CO_2 has been reported to improve the C_{2+} selectivity and reduce the CH_4 conversion.[38,51,52] For example, MgO or Sm_2O_3-based catalysts exhibited increased C_{2+} selectivity with a low partial pressure of CO_2.[32,53] Suppressed OCM activity with CO_2 has also been reported: Li/MgO was poisoned by CO_2,[54] and Na_2WO_4/Mn/SiO_2 was deactivated by concentrated CO_2.[38] Nevertheless, it may be possible to modify the OCM activity by using an appropriate amount of co-fed CO_2 as mild oxidant to replace the mixture of N_2 and O_2. Thus, the OCM reaction was tested at a fixed feed flow rate, variable catalyst bed thickness, and the 20% N_2 in the feed was replaced by 16% CO_2 + 4% N_2 in order to investigate this possibility and understand the effects of the adsorbed oxygen atoms (Fig. 6, S6, Tables S7 and S8†).

When increasing the catalyst bed thickness (or decreasing the GHSV), CH_4 conversion and C_{2+} selectivity reached 30.8–34.5% and 51.1–61.9%, respectively at 100% O_2 conversion
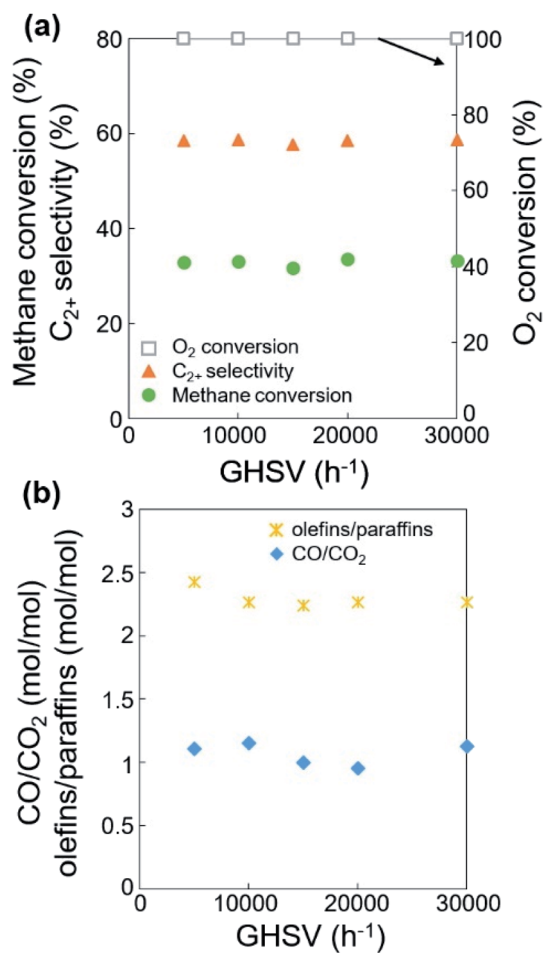

Fig. 6   (a) Catalytic activities, (b) ratios of olefins/paraffins and CO/CO_2, and (c) oxygen consumption for the dehydrogenation of ethane (or propane) and the oxidation of CO, depending on the catalyst bed thickness at CH_3/O_2/N_2/CO_2 = 3/1/0.2/0.8 mol/mol/mol/mol and 800 °C.

(Table S5†), which is similar to the results using N_2 as diluent (32.1–35.9% and 50.9–59.8%, respectively, Table S3†). Compared with the use of N_2 diluent, the co-feeding of CO_2 slightly lowered CH_4 conversion and slightly improved C_{2+} selectivity by 1.5–4.7%, achieving almost identical C_{2+} yields. The improved C_{2+} selectivity was more distinct when the O_2 was not completely consumed (O_2 conversion < 100%), particularly when GHSV >20 000 h^{-1} at 750 °C.

In terms of the selectivity between CO and CO_2, a larger CO/CO_2 ratio was observed when CO_2 was co-fed compared to using the N_2 diluent alone (Tables S3 and S7†). The improved formation of CO with CO_2 co-feeding can be attributed to the catalytic conversion of CO_2 to CO. While this conversion can occur by either the reduction or catalytic dissociation of CO_2, a highly oxidizing environment can suppress the reduction reaction by hydrogen generated in the dehydrogenation of paraffin or reduction of water. The catalytic dissociation of CO_2 to CO and O may occur to increase the concentration of CO,[50,51] and the produced oxygen atoms may improve the C_{2+} selectivity.
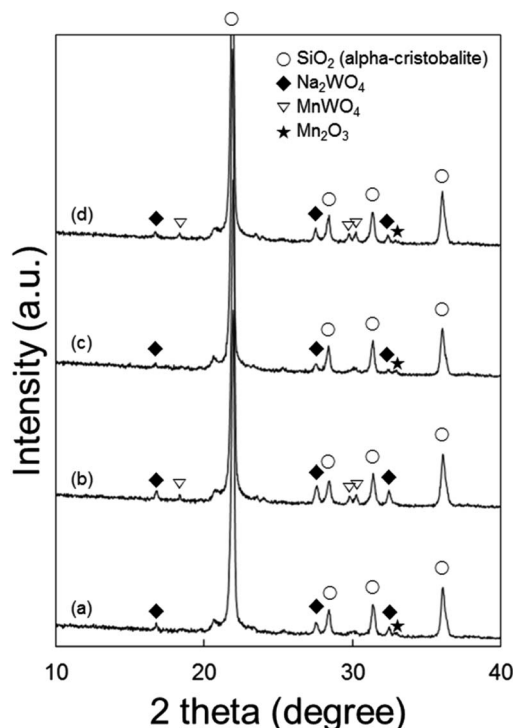
Fig. 7 XRD results of $Na_2WO_4/Mn/SiO_2$ spent in the reaction with N_2 diluent from the (a) top and (b) bottom of the catalyst bed, and in the reaction with co-fed CO_2 from the (c) top and (d) bottom of the catalyst bed. The peaks were assigned to α-cristobalite SiO_2 (○), Na_2WO_4 (◆), $MnWO_4$ (▽), and Mn_2O_3 (★).

The actual temperatures of the top, middle, and bottom layers of the 35.3 mm catalyst bed were measured (Fig. S2†). The temperature was observed to decrease from the top to the bottom layer, indicating that the involved reactions occurred at the entrance of the catalyst bed.

We also summarized all the reaction results obtained in this study in terms of C_{2+} yield, depending on CH_4 conversion and O_2 conversion (Fig. S7†). Regardless of reaction conditions, CH_4 conversion, O_2 conversion (for <100%), and C_{2+} yield increased proportionally with each other, indicating that the formation of C_{2+} compounds was not significantly adjusted by varying the reaction conditions, as long as O_2 was present. Thus, the effects of surface lattice oxygen species may not be significant while O_2 is present.

3.4. Identification of crystal structures

To understand the effects of catalyst structures on the OCM activity, the spent catalysts were characterized (Fig. 7). There was no significant difference between catalysts spent using N_2 as diluent alone and with CO_2 co-feeding. However, when using a longer catalyst bed or smaller GHSV, catalysts on the top and bottom of the bed exhibited different structures. The formation of $MnWO_4$ was distinct at the bottom (O_2-deficient region) but not clearly observed at the top (O_2-rich region). While $MnWO_4$ had been reported in the literature as either an active or inactive component,[22,28,47,55,56] we observed moderate OCM activity on
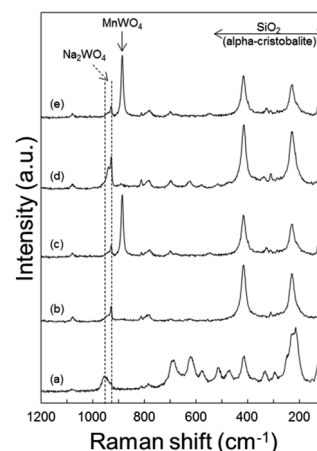

Fig. 8 Raman spectra of $Na_2WO_4/Mn/SiO_2$ catalyst: (a) in the fresh state, after the reaction with N_2 diluent at the (b) top and (c) bottom of the catalyst bed, after the reaction with co-fed CO_2 at the (d) top and (e) bottom of the catalyst bed.

$MnWO_4$ powder (Fig. S9†). While the co-existing Na_2WO_4 and α-cristobalite SiO_2 are known as key components for good OCM catalysts,[22,23,57] it is not clear whether the formation of $MnWO_4$ reduced the OCM activity or not in this study.

When heated to 800 °C in air, the Na_2WO_4 and Mn_2O_3 phases were found to disappear for the fresh catalyst at room temperature, indicating the melting of these solid materials (Fig. S8(a)†). Compared to these, $MnWO_4$ survived, while maintaining its solid structure at the OCM reaction temperature. α-Cristobalite SiO_2 exhibited a peak shift toward smaller 2θ or larger d-spacings, indicating thermal expansion of the crystal structure.

3.5. Study of catalyst surface by Raman spectroscopy and XPS

Raman spectra of the spent catalysts also confirmed the formation of $MnWO_4$ in the O_2-deficient region (bottom layer of catalyst bed) by the distinct $MnWO_4$ peak at 885 cm^{-1} for both CO_2-free and CO_2-added feeds (Fig. 8). Raman bands indicating Na_2WO_4 were observed in the fresh catalyst and spent ones at all regions of the bed. Notably, the bands at or below 500 cm^{-1} can be attributed to α-cristobalite SiO_2, and those at 500–700 cm^{-1} can be attributed to manganese oxides.[24] When heated to 800 °C in air, Mn_2O_3 and α-cristobalite SiO_2 peaks became weaker than those of the fresh catalyst, indicating that these phases became weaker or less ordered at high temperatures (Fig. S8(b)†).

In terms of surface electronic structures, the spent catalysts exhibited more intense Na 1s and Mn 2p peaks when only N_2 was used as diluent in the reaction (Table S9†). The O 1s peaks at 530.9 eV indicating the presence of Na_2WO_4 were stronger than those with co-fed CO_2 (Fig. S10†). The peaks at 532.6 eV are assigned to SiO_2. Compared to the fresh catalyst, the spent catalysts after reaction with N_2 as the only diluent or with co-fed CO_2 had much higher surface concentrations of Mn as measured by XPS (Table S9†). This growing surface concentration of Mn can be attributed to the formation of $MnWO_4$, even

Table 2 OCM results using spent catalyst prepared in the O_2-deficient region (bottom of catalyst bed)[a,b]

Reaction temperature (°C)	$X(CH_4)$ (%)	$X(O_2)$ (%)	$S(C_{2+})$ (%)	$Y(C_{2+})$ (%)	Olefins/paraffins (mol mol^{-1})
Fresh Na$_2$WO$_4$/Mn/SiO$_2$					
750	35.2	100	54.5	19.2	2.12
800	35.3	100	51.5	18.2	2.49
850	33.4	100	45.9	15.4	3.77
Spent Na$_2$WO$_4$/Mn/SiO$_2$ prepared in the O$_2$-deficient region					
750	35.0	98.2	59.6	20.8	2.11
800	35.8	100	53.4	19.1	2.68
850	34.1	100	49.9	17.0	3.98

[a] GHSV = 10 000 h^{-1}, $CH_4/O_2/N_2$ = 3/1/1 mol/mol/mol, total feed flow rate = 30 mL min^{-1}. [b] $X(CH_4)$: CH_4 conversion, $X(O_2)$: O_2 conversion, $S(C_{2+})$: C_{2+} selectivity, $Y(C_{2+})$: C_{2+} yield.

though the distinct peaks could not be identified because the Mn may have protruded to the surface by complexation with W species.[47]

The spent catalyst from the O_2-deficient region (which exhibited the formation of $MnWO_4$) was re-used for the OCM, and the activity was compared with the fresh one (Table 2). The spent catalyst exhibited higher C_{2+} selectivity, higher C_{2+} yield, and higher olefins/paraffins ratio by 3.7–9.4%, 4.9–10.4%, and 0–7.6%, respectively. Therefore, the spent catalysts containing $MnWO_4$ produced more C_{2+} compounds along with a higher dehydrogenation activity. These observations confirmed that dehydrogenation occurred preferably in the O_2-deficient region, which exhibited the formation of $MnWO_4$.

4. Conclusions

The catalytic oxidative coupling of methane to C_{2+} compounds was examined under various reaction conditions, and the following results were obtained.

(i) Oxygen species formed by the adsorption of gas-phase O_2 preferentially activated methane molecules to produce methyl radicals, while those formed by the diffusion of bulk lattice oxygen atoms preferred the dehydrogenation of paraffins to olefins.

(ii) The co-feeding of CO_2 slightly increased the C_{2+} selectivity compared to the reaction without CO_2 co-feeding; however, no significant improvement was observed exhibiting almost identical C_{2+} yield, although beneficial effects have been reported.

(iii) The formation of $MnWO_4$ on the catalyst was improved in the O_2-free environment at the O_2-deficient bottom of the catalyst bed, which exhibited the preferred dehydrogenation reaction. This also confirmed the diffusion of bulk lattice oxygen atoms to the catalyst surface.

In this study, we focused on the OCM reaction in the non-steady states. The roles of surface lattice oxygen atoms and the reaction-initiated changes in the catalyst bed were clearly observed. Those results will help researchers and engineers understand the scaled-up OCM processes for the conversion of methane to paraffins and olefins.

Conflicts of interest

There are no conflicts to declare.

Acknowledgements

Notes and references

1 S. Lim, J.-W. Choi, D. J. Suh, K. H. Song, H. C. Ham and J.-M. Ha, *J. Catal.*, 2019, **375**, 478–492.

2 B. L. Farrell, V. O. Igenegbai and S. Linic, *ACS Catal.*, 2016, **6**, 4340–4346.

3 J. C. W. Kuo, C. T. Kresge and R. E. Palermo, *Catal. Today*, 1989, **4**, 463–470.

4 A. M. Maitra, *Appl. Catal., A*, 1993, **104**, 11–59.

5 J. H. Lunsford, *Angew. Chem., Int. Ed.*, 1995, **34**, 970–980.

6 U. Zavyalova, M. Holena, R. Schlogl and M. Baerns, *ChemCatChem*, 2011, **3**, 1935–1947.

7 Y. S. Su, J. Y. Ying and W. H. Green, *J. Catal.*, 2003, **218**, 321–333.

8 A. Cruellas, J. J. Bakker, M. V. Annaland, J. A. Medrano and F. Gallucci, *Energy Convers. Manage.*, 2019, **198**, 111789.

9 N. S. Hayek, G. J. Khlief, F. Horani and O. M. Gazit, *J. Catal.*, 2019, **376**, 25–31.

10 S. Arndt, G. Laugel, S. Levchenko, R. Horn, M. Baerns, M. Scheffler, R. Schlögl and R. Schomäcker, *Catal. Rev.*, 2011, **53**, 424–514.

11 J. M. DeBoy and R. F. Hicks, *Ind. Eng. Chem. Res.*, 1988, **27**, 1577–1582.

12 S. Lim, J.-W. Choi, D. Jin Suh, U. Lee, K. H. Song and J.-M. Ha, *Catal. Today*, 2020, **352**, 127–133.

13 G. Lee, I. Kim, I. Yang, J.-M. Ha, H. B. Na and J. C. Jung, *Appl. Surf. Sci.*, 2018, **429**, 55–61.

14 D. Kwon, I. Yang, Y. Sim, J.-M. Ha and J. C. Jung, *Catal. Commun.*, 2019, **128**, 105702.

15 Y. Sim, J. Yoo, J.-M. Ha and J. C. Jung, *J. Energy Chem.*, 2019, **35**, 1–8.

16 S.-B. Li, *Chin. J. Chem.*, 2001, **19**, 16–21.

17 U. Simon, O. Gorke, A. Berthold, S. Arndt, R. Schomacker and H. Schubert, *Chem. Eng. J.*, 2011, **168**, 1352–1359.

18 S. Pak and J. H. Lunsford, *Appl. Catal., A*, 1998, **168**, 131–137.

19 H. R. Godini, A. Gili, O. Gorke, U. Simon, K. Hou and G. Wozny, *Energy Fuels*, 2014, **28**, 877–890.

20 V. Fleischer, R. Steuer, S. Parishan and R. Schomacker, *J. Catal.*, 2016, **341**, 91–103.

21 S. Li, *J. Nat. Gas Chem.*, 2003, **12**, 1–9.

22 S. Arndt, T. Otremba, U. Simon, M. Yildiz, H. Schubert and R. Schomäcker, *Appl. Catal., A*, 2012, **425–426**, 53–61.

23 A. Palermo, J. P. Holgado Vazquez, A. F. Lee, M. S. Tikhov and R. M. Lambert, *J. Catal.*, 1998, **177**, 259–266.

24 S.-F. Ji, T.-C. Xiao, S.-B. Li, C.-Z. Xu, R.-L. Hou, K. S. Coleman and M. L. H. Green, *Appl. Catal., A*, 2002, **225**, 271–284.

25 J. G. Wu and S. B. Li, *J. Phys. Chem.*, 1995, **99**, 4566–4568.

26 Y. Kou, B. Zhang, J.-z. Niu, S.-b. Li, H.-l. Wang, T. Tanaka and S. Yoshida, *J. Catal.*, 1998, **173**, 399–408.

27 D. J. Wang, M. P. Rosynek and J. H. Lunsford, *J. Catal.*, 1995, **155**, 390–402.

28 S. Ji, T. Xiao, S. Li, L. Chou, B. Zhang, C. Xu, R. Hou, A. P. E. York and M. L. H. Green, *J. Catal.*, 2003, **220**, 47–56.

29 S. Gu, H. S. Oh, J. W. Choi, D. J. Suh, J. Jae, J. Choi and J. M. Ha, *Appl. Catal., A*, 2018, **562**, 114–119.

30 J. S. Chang, V. P. Vislovskiy, M. S. Park, D. Y. Hong, J. S. Yoo and S. E. Park, *Green Chem.*, 2003, **5**, 587–590.

31 X. H. Li, K. Tomishige and K. Fujimoto, *Catal. Lett.*, 1996, **36**, 21–24.

32 T. Nishiyama and K.-I. Aika, *J. Catal.*, 1990, **122**, 346–351.

33 C. L. Chen, Y. D. Xu, G. J. Li and X. X. Guo, *Catal. Lett.*, 1996, **42**, 149–153.

34 S. Alzahrani, Q. Song and L. L. Lobban, *Ind. Eng. Chem. Res.*, 1994, **33**, 251–258.

35 K.-i. Aika and T. Nishiyama, *J. Chem. Soc., Chem. Commun.*, 1988, 70–71, DOI: 10.1039/C39880000070.

36 S. J. Korf, J. A. Roos, N. A. de Bruijn, J. G. van Ommen and J. R. H. Ross, *J. Chem. Soc., Chem. Commun.*, 1987, 1433–1434, DOI: 10.1039/C39870001433.

37 J. Shi, L. Yao and C. W. Hu, *J. Energy Chem.*, 2015, **24**, 394–400.

38 J. Shi, L. Yao and C. Hu, *J. Energy Chem.*, 2015, **24**, 394–400.

39 J. Y. Lee, W. Jeon, J.-W. Choi, Y.-W. Suh, J.-M. Ha, D. J. Suh and Y.-K. Park, *Fuel*, 2013, **106**, 851–857.

40 R. M. Freire, F. F. de Sousa, A. L. Pinheiroa, E. Longhinotti, J. Mendes, A. C. Oliveira, P. D. C. Freire, A. P. Ayala and A. C. Oliveira, *Appl. Catal., A*, 2009, **359**, 165–179.

41 J. S. Yoo, P. S. Lin and S. D. Elfline, *Appl. Catal., A*, 1993, **106**, 259–273.

42 J. Wang, L. Chou, B. Zhang, H. Song, J. Zhao, J. Yang and S. Li, *J. Mol. Catal. A: Chem.*, 2006, **245**, 272–277.

43 V. O. Igenegbai, R. J. Meyer and S. Linic, *Appl. Catal., B*, 2018, **230**, 29–35.

44 T. P. Tiemersma, M. J. Tuinier, F. Gallucci, J. A. M. Kuipers and M. v. S. Annaland, *Appl. Catal., A*, 2012, **433–434**, 96–108.

45 M. R. Lee, M. J. Park, W. Jeon, J. W. Choi, Y. W. Suh and D. J. Suh, *Fuel Process. Technol.*, 2012, **96**, 175–182.

46 W. Jeon, J. Y. Lee, M. Lee, J.-W. Choi, J.-M. Ha, D. J. Suh and I. W. Kim, *Appl. Catal., A*, 2013, **464–465**, 68–77.

47 R. T. Yunarti, S. Gu, J.-W. Choi, J. Jae, D. J. Suh and J.-M. Ha, *ACS Sustainable Chem. Eng.*, 2017, **5**, 3667–3674.

48 S. Gu, H.-S. Oh, J.-W. Choi, D. J. Suh, J. Jae, J. Choi and J.-M. Ha, *Appl. Catal., A*, 2018, **562**, 114–119.

49 C. Karakaya, H. Y. Zhu, C. Loebick, J. G. Weissman and R. J. Kee, *Catal. Today*, 2018, **312**, 10–22.

50 T. Yabe and Y. Sekine, *Fuel Process. Technol.*, 2018, **181**, 187–198.

51 Y. Liu, J. Xue, X. Liu, R. Hou and S. Li, in *Stud. Surf. Sci. Catal.*, ed. D. S. F. F. A. V. A. Parmaliana and F. Arena, Elsevier, 1998, vol. 119, pp. 593–597.

52 Y. Liu, R. L. Hou, X. X. Liu, J. Z. Xue and S. B. Li, in *Natural Gas Conversion V*, ed. A. Parmaliana, D. Sanfilippo, F. Frusteri, A. Vaccari and F. Arena, Elsevier Science Publ B V, Amsterdam, 1998, vol. 119, pp. 307–311.

53 S. Kuś, M. Otremba, A. Tórz and M. Taniewski, *Appl. Catal., A*, 2002, **230**, 263–270.

54 K. P. Peil, J. G. Goodwin Jr and G. Marcelin, *J. Catal.*, 1991, **131**, 143–155.

55 S. Sadjadi, S. Jaso, H. R. Godini, S. Arndt, M. Wollgarten, R. Blume, O. Gorke, R. Schomacker, G. Wozny and U. Simon, *Catal. Sci. Technol.*, 2015, **5**, 942–952.

56 T. W. Elkins and H. E. Hagelin-Weaver, *Appl. Catal., A*, 2015, **497**, 96–106.

57 Z. C. Jiang, C. J. Yu, X. P. Fang, S. B. Li and H. L. Wang, *J. Phys. Chem.*, 1993, **97**, 12870–12875.